A&A 419, 375–383 (2004)
DOI: 10.1051/0004-6361:20040073

Astronomy & Astrophysics

The nuclei of comets 126P/IRAS and 103P/Hartley 2⋆

O. Groussin[1,⋆⋆], P. Lamy[1], L. Jorda[1], and I. Toth[1,2]

[1] Laboratoire d'Astronomie Spatiale, BP 8, 13376 Marseille Cedex 12, France
[2] Konkoly Observatory, PO Box 67, Budapest 1525, Hungary

Received 6 May 2003 / Accepted 15 January 2004

Abstract. We report the detection of the nucleus of 126P/IRAS and 103P/Hartley 2 with the Infrared Camera of the Infrared Space Observatory (ISOCAM). 126P/IRAS was observed on 12 November 1996, when it was at r_h = 1.71 AU from the Sun and Δ = 1.32 AU from the Earth. 103P/Hartley 2 was observed on 5 February 1998, when it was at r_h = 1.21 AU from the Sun and Δ = 0.91 AU from the Earth. The observations were performed with the broadband LW10 filter centered at 11.5 μm. The spatial resolution was adequate to separate the thermal emission of the nuclei from that of their respective comae. We combined the ISOCAM observations with measured water production rates, using a model that considers a spherical nucleus with a macroscopic mosaic of small and numerous active and inactive regions, and we derived a radius of 1.57 ± 0.14 km and an active fraction at perihelion of 0.11 ± 0.03 for 126P/IRAS, and a radius of 0.71 ± 0.13 km and an active fraction of ∼1 at perihelion and 0.30 ± 0.11 at 1.11 AU post-perihelion for 103P/Hartley 2. These two examples illustrate the large diversity of activity pattern that exists among cometary nuclei.

Key words. comets: individual: 126P/IRAS – comets: individual: 103P/Hartley 2 – comets: general

1. Introduction

The knowledge and the understanding of the physical properties of cometary nuclei are important to constrain their origin and their evolution in the solar system. In the past ten years there has been major progress in the characterization of a large number of cometary nuclei by several groups using different techniques (see the recent review by Lamy et al. 2004). Our own technique relies on the high spatial resolution offered by space observatories, the Hubble Space Telescope (HST) in the visible and the Infrared Space Telescope (ISO) in the thermal infrared, to detect a cometary nucleus even when it is active, i.e., in the presence of its surrounding coma. In several instances, we have been able to detect nuclei in both visible and infrared spectral domains, thus determining their radius and albedo independently: C/1995 O1 Hale-Bopp (Lamy et al. 1999; Weaver & Lamy 1999), 22P/Kopff (Lamy et al. 2002) and 55P/Tempel-Tuttle (Lamy et al. 2004). In this article, we present an extensive analysis of two active nuclei, that of comet 126P/IRAS and that of comet 103P/Hartley 2, which have been detected only in the thermal infrared with ISO. Technical details of these observations as well as preliminary results have already been published (Jorda et al. 2000). Our present analysis includes the constraints from the water production rates and allows for the first time the self-consistent determination of the size and active fraction of the nucleus.

Comet 126P/IRAS was detected by Davies et al. (1983) with the Infrared Astronomy Satellite IRAS on 26 April 1983, thanks to a close approach to Earth ($\Delta \sim 0.78$ AU). It is a Nearly Isotropic Comet according to the classification of Levison (1996) and its orbital evolution is presently controlled by close approaches to Saturn (Carusi et al. 1985). The approach of 1950 led to abrupt changes of its Tisserand invariant relative to Jupiter and of its perihelion distance (from ∼2 AU to ∼1.7 AU). The other orbital parameters are quite stable except for a slight periodic variation of the aphelion distance.

Comet 103P/Hartley 2 is an Ecliptic Comet (Levison 1996) discovered on 28 November 1984 by Hartley (1984). It moved in the vicinity of the 1:1 mean motion resonance (MMR) with Jupiter so that its orbit did not vary much until ∼1875. Then a succession of encounters with Jupiter put it slightly above the 2:1 MMR, drastically reducing its perihelion (from ∼2.9 AU to ∼1 AU) and aphelion distances (from ∼8 AU to ∼6 AU; Carusi et al. 1985). It is one of the few comets that have become Earth crossers in the recent past.

The present orbital parameters of the two comets are presented in Table 1.

2. Observations and preprocessing of the images

The two comets were imaged with the LW (long wavelength) channel of ISOCAM, the infrared camera aboard ISO

Send offprint requests to: O. Groussin,
e-mail: grousssin@astro.umd.edu

⋆ Based on observations made with the Infrared Space Observatory, an ESA project with instruments funded by ESA Member States (especially the PI countries: France, Germany, The Netherlands and UK) and with the participation of ISAS and NASA.

⋆⋆ *Present address:* Department of Astronomy, University of Maryland, College Park, MD 20742-2421, USA.

Table 1. Orbital elements of the observed comets.

Comet	T_J^a	P_{orb}^b [year]	q^c [AU]	Q^d [AU]	e^e	i^f [°]
126P/IRAS	1.96	13.16	1.703	9.538	0.697	46.0
103P/Hartley 2	2.64	6.39	1.032	5.871	0.701	13.6

[a] Tisserand parameter relative to Jupiter; [b] orbital period; [c] perihelion distance; [d] aphelion distance; [e] eccentricity; [f] inclination.

(Cesarsky 1994; Cesarsky et al. 1996) using the LW10 filter and the mode offering the highest spatial resolution of 1.5 arcsec pixel^{-1}. LW10 is a broadband filter centered at 11.5 μm with a *FWHM* of 7 μm.

The observations of 126P/IRAS were performed on a single day, 12 November 1996, 13 days after its perihelion passage of 30 October 1996. The observing programme consisted of seven visits spanning a time interval of 10 h. The geometric parameters varied only slightly over this interval: the heliocentric distance r_h changed from 1.7077 to 1.7081 AU and the geocentric distance Δ from 1.3162 to 1.3210 AU, resulting in a negligible increase of the image scale, from 1432 to 1437 km pixel^{-1}. The solar phase angle α remained nearly constant at 35.3°.

Comet 103P/Hartley 2 passed perihelion on 21 December 1997 and was closest to Earth on 8 January 1998 at Δ = 0.8177 AU. Operational constraints of ISO pushed the observation to 5 February 1998, that is 46 days after its perihelion passage. The observing program consisted of three visits spanning a time interval of 20 min. The geometric parameters remained nearly constant over such a short interval: r_h = 1.2091 AU, Δ = 0.9084 AU, α = 53.2° and the pixel scale amounted to 988 km pixel^{-1}.

Because of the particular operation of the infrared detectors, two parameters were needed to define an exposure: the individual exposure time and the number of individual frames. The first parameter equal to 2.1 s was selected to maximize the signal without saturating the detector. The second parameter ensured that, after a phase of stabilization of the detector, an adequate number of scientific frames were accumulated to reach the desired signal-to-noise ratio. This parameter amounted to 20 and 85 individual frames for respectively, 126P/IRAS and 103P/Hartley 2.

The accuracy of the pointing was limited by the capability of ISO, the specification being a 2σ error of 11.7 arcsec. The nucleus of 126P/IRAS landed 3.2 arcsec away from the center of the frame (~2.1 pixels) while that of 103P/Hartley 2 landed 11.0 arcsec away from the center (~7.3 pixels). ISOCAM observations of moving targets were obtained in "tracking mode" with the satellite performing a one-dimensional micro-raster along the apparent trajectory of the target. Thus, one observation consisted of multiple pointings, each of them referred to as a raster point, to correct for cometary motion. In a separate program devoted to observations of comet Hale-Bopp, we carried out a detailed analysis of the pointing history file and found that the comet was 95 percent of the time within 0.49 arcsec ($\simeq$1/3 pixel) from the averaged raster position (Jorda et al. 2000).

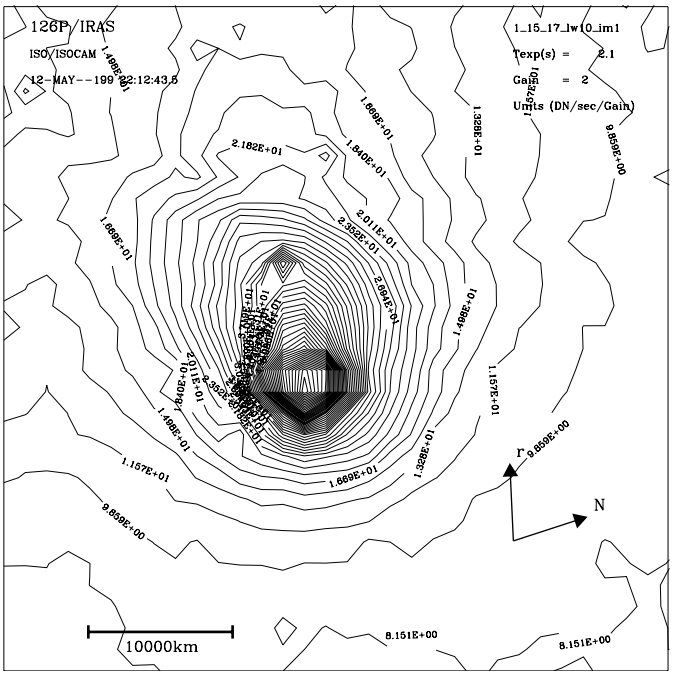

Fig. 1. Isophote contours of an image of comet 126P/IRAS taken on 12 November 1996 with the LW10 filter of ISOCAM. The arrows indicate the anti-solar direction (prolonged radius vector ***r***) and the direction of the celestial (equatorial) North (N). There is a star in the anti-solar direction.

An ISOCAM image is in fact a cube where the additional dimension is time. The signal in a given pixel (i, j) is indeed a function of time (t_k) for reasons explained above. The preprocessing of the cubes is rather complex and thoroughly described by Jorda et al. (2000). In summary, the corrections for dark current, non-uniformities and transient effects used the tools of the CAM Interactive Analysis Software (CIA version 3.0). However we developed a specific IDL (Interactive Data Language) routine to select the valid images and combine them in the most appropriate way. It examines how fast the stabilization takes place and looks for overshoots in each individual pixel. The latter problem arises when the signal does not smoothly reach its maximum value but first overshoots it before leveling off to the true "stabilized value". The absolute calibration was performed using the most recent factors (Siebenmorgen et al. 1998) and applying an appropriate color correction (Siebenmorgen et al. 1999). The adopted calibration factors are given by Jorda et al. (2000) in their Table 3. Figure 1 displays an image of 126P/IRAS created from 20 individual exposures of 2.1 s while Fig. 2 displays an image of 103P/Hartley created from 85 individual exposures of 2.1 s with the method described by Jorda et al. (2000). At this stage, seven (for 126P) and three (for 103P) such calibrated images (one per visit) were available for analysis.

3. Image analysis

The separation of the nucleus and coma signals must be accurately performed in order to retrieve the correct flux of the nucleus. The best approach consists of fitting a parametric model

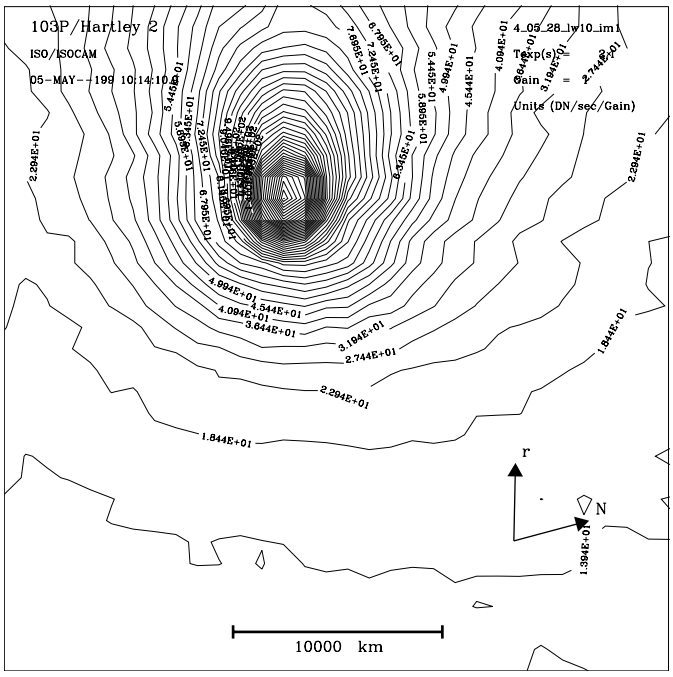

Fig. 2. Isophote contours of an image of comet 103P/Hartley 2 taken on 5 February 1998 with the LW10 filter of ISOCAM. The arrows indicate the anti-solar direction (prolonged radius vector $\boldsymbol{r}$) and the direction of the celestial (equatorial) North (N).

of the expected surface brightness to the observed images. The most general model represented by a 2-dimensional array of brightness values is simply given by

$$\text{Model} = [\text{nucleus} + \text{coma}] \otimes PSF, \quad (1)$$

where $\otimes$ represents the convolution operator and PSF denotes the point spead function of the telescope (the required PSFs come from a library compiled by the ISOCAM team as described by Lamy et al. 2002). The nucleus is not resolved so that

$$\text{nucleus} = k_{\rm n}\, \delta(\rho), \quad (2)$$

where δ is the Dirac delta function, ρ is the radial distance from the center and $k_{\rm n}$ is a scaling factor. Specifying a model for the coma very much depends on how complex it appears on the real images and we developed various models accordingly. In the two cases here, the innermost coma appears to slightly depart from circular symmetry but not to the point of warranting the most general procedure we implemented for comet Hale-Bopp (Weaver & Lamy 1999). We therefore decided to introduce the isotropic model

$$\text{coma} = k_{\rm c} \,/\, \rho^{p} \quad (3)$$

and to perform the fits on azimuthally averaged radial profiles as we did for instance for comet 46P/Wirtanen (Lamy et al. 1998a). This was implemented by performing a polar transformation of the images centered on the nucleus (the pixel having the largest signal) with an angular resolution of 1° and summing only 270 individual profiles out of 360. This excludes the quadrant centered along the anti-solar direction so as to avoid

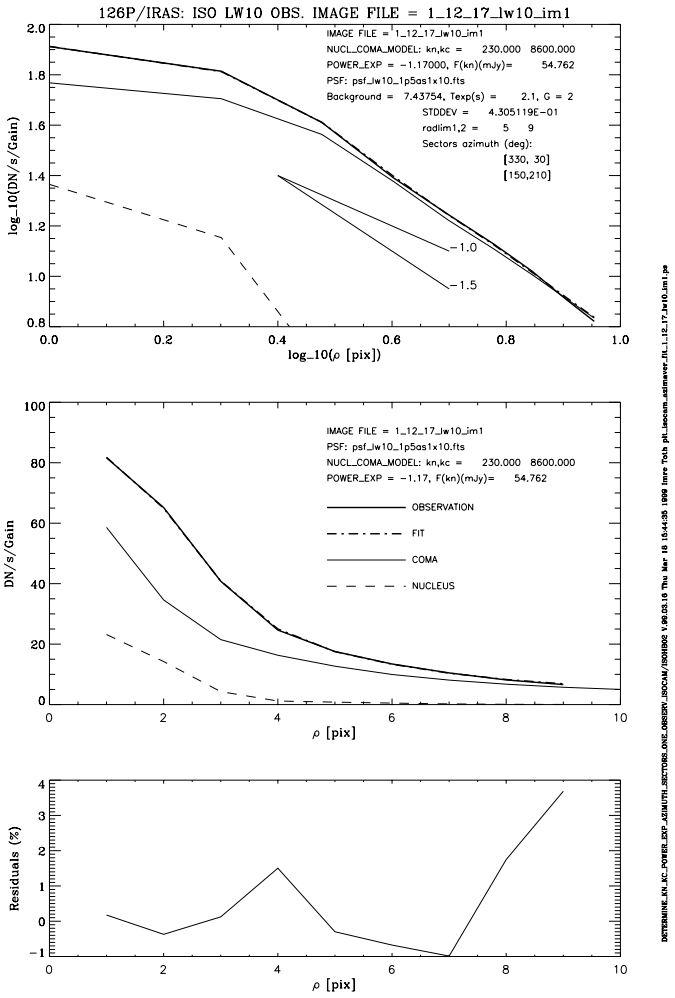

Fig. 3. Azimuthally averaged radial profile of an image of 126P/IRAS in log–log (*top*) and linear-linear (*middle*) representations. The lower panel displays the residuals of the fit.

the tailward distortion of the coma (as well as a star in the case of 126P). Note that the $1/\rho^{p}$ function was rigorously calculated in the central 3×3 pixels to take into account the finite extent of the pixels (this effect is negligible beyond).

Figure 3 illustrates the result of the best fit for an image of 126P/IRAS. Note the ability of the model to reproduce the observation at the level of ±1% in the region of interest. In the central pixel, the contribution of the nucleus amounts to ∼25% of the total signal, while it was ∼18% in the case of our ISOCAM observations of comet 22P/Kopff (Lamy et al. 2002). The power exponent of the inner coma $p = -1.17$ deviates from the canonical value and indicates that it was not in steady state.

Figure 4 illustrates the result of the best fit for an image of 103P/Hartley 2. The contribution of the nucleus is quite small, only ∼8% of the total signal in the central pixel. Still the model is able to reveal it, although with a large uncertainty (see below) and the fit is good at the level of ±2% in the region of interest. With a power exponent of $p = -1.05$, the inner coma was very close to steady state.

Our results are summarized in Table 2. There are several sources of noise in the ISOCAM images which are fully

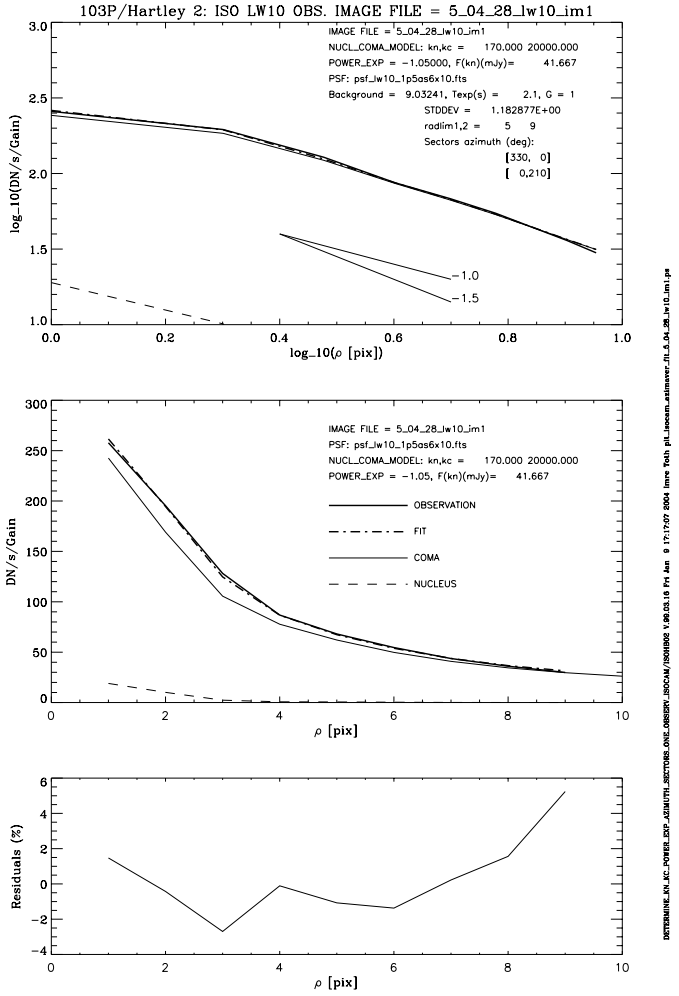

Fig. 4. Azimuthally averaged radial profile of an image of 103P/Hartley 2. See Fig. 3 for explanations.

discussed in our study of 22P/Kopff (Lamy et al. 2002). Altogether, the non-systematic errors (flat-field subtraction, dark current subtraction, transient correction, photon noise) lead to a typical 1-σ error of ∼16%. For 126P, the dispersion of the flux values around the average of 48 mJy amounts to ±8 mJy, that is 16.7%, in agreement with the above determination. The situation is less favorable for 103P as the subtraction of the overhelming coma introduces a further, non-neglible source of uncertainty fully reflected by the large dispersion of the flux values. We take the average of the three determinations and their full dispersion to quantify the uncertainty and obtain 27 ± 15 mJy, that is an error of ±57%, not untypical of infrared observations of weak sources. Finally, the systematic error on the absolute calibration was estimated by Siebenmorgen et al. (1998) to be ∼5%.

4. The model of the nucleus

The interpretation of the ISOCAM infrared observations requires a thermal model of the nucleus. Traditionally, the Standard Thermal Model (Lebofsky et al. 1986) is applied to derive the nucleus radius (e.g., Lisse et al. 1999; Fernandez et al. 2000; Jorda et al. 2000), and then an active area is derived from this radius, using the water production rates (A'Hearn et al. 1995). But this suffers from the paradox that the STM was developed for asteroids and does not take into account water ice on the surface, in contradiction to the activity observed on comets. Consequently, we developed a model, in the framework of that of Crifo & Rodionov (1997), that takes into account the presence of water ice on the surface, through active regions. This model is applied simultaneously to the infrared observations and the measured water production rates, to determine, in a self-consistent way, the nucleus radius and its active fraction. This is the first time that such a method is implemented.

Table 2. Journal of the ISOCAM observations and results.

Image	Date[a] [UT]	τ^b [s]	G^c	Flux[d] [mJy]
126P/IRAS r_h = 1.71 AU Δ = 1.32 AU α = 35°				
1_09_17_lw10	1996 Nov. 12.50797	2.1	2	43
1_10_17_lw10	1996 Nov. 12.57868	2.1	2	48
1_11_17_lw10	1996 Nov. 12.65295	2.1	2	60
1_12_17_lw10	1996 Nov. 12.72146	2.1	2	55
1_13_17_lw10	1996 Nov. 12.79132	2.1	2	36
1_14_17_lw10	1996 Nov. 12.85413	2.1	2	50
1_15_17_lw10	1996 Nov. 12.92551	2.1	2	43
				48 ± 8*
103P/Hartley 2 r_h = 1.21 AU Δ = 0.91 AU α = 53°				
5_04_28_lw10	1998 Feb. 5.45350	2.1	1	27
4_05_28_lw10	1998 Feb. 5.42652	2.1	1	13
4_06_28_lw10	1998 Feb. 5.44001	2.1	1	42
				27 ± 15*

[a] Exposure mid-point; [b] exposure time; [c] gain; [d] flux of the nucleus (at 11.5 μm); * average flux.

4.1. The thermal model

Our model is a mosaic of active and inactive regions on a spherical nucleus, already used for 22P/Kopff (Lamy et al. 2002) and 46P/Wirtanen (Groussin et al. 2003a). Active regions are small, numerous, and located all over the nucleus to be consistent with the absence of structure (jets) in the coma. The fraction of the surface x covered by active region ranges from 0 (nucleus 100% inactive) to 1 (nucleus 100% active), and is called the active fraction. Active regions are a microscopic mixture of water ice and refractory materials. The volumic fraction of water ice in this mixture f ranges from 0 (no water ice) to 1 (pure water ice). We take into account all first order physical processes, insolation, radiation and water ice sublimation and neglect heat conduction for reasons given below

Heat conduction is linked to the thermal inertia I, which we expressed in MKS unit, that is J/K/m^2/s$^{1/2}$. It has been determined for a few small bodies in the Solar System: I < 15 MKS for main-belt asteroids (Spencer et al. 1989), ≤10.5 MKS for Centaur Asbolus (Fernandez et al. 2002), ∼3 MKS and ∼0 MKS respectively for Centaurs Chiron and Chariklo (Groussin et al. 2004). So, the thermal inertia of

cometary nuclei is certainly very low, probably in the range 0–20 MKS. For cometary nuclei with such a low thermal inertia and that are further observed at short heliocentric distances $r_h < 2$ AU, we have already shown that the heat conduction has no influence on the determination of the radius of the nucleus (Groussin 2003b). We checked this result for the two comets of interest here and indeed found that the effect of the thermal inertia in the range 0–20 MKS on the radius determination is less than 1%; it can therefore be safely neglected.

The low conductivity of the nucleus further ensures that there is no thermal coupling between active and inactive regions. Each region has its own surface temperature given by the surface energy balance, for an inactive region:

$$(1-A)\frac{F_{\rm sun}}{r_{\rm h}^2}\cos z = \eta\epsilon\sigma T^4 \quad (4)$$

and for an active region:

$$(1-A)\frac{F_{\rm sun}}{r_{\rm h}^2}\cos z = \eta\epsilon\sigma T^4 + f(1-\alpha_{\rm R})LZ(T) \quad (5)$$

where $A = p_{\rm v}q$ is the product of the geometric albedo $p_{\rm v}$ by the phase integral q, $F_{\rm sun}$ [W m^{-2}] is the solar constant at 1 AU, $r_{\rm h}$ [AU] is the heliocentric distance, z is the zenithal angle, η is the beaming factor introduced by Lebofsky et al. (1986), ϵ is the infrared emissivity, σ [J K^{-4} m^{-2} s^{-1}] is the Stefan-Boltmann's constant, T [K] is the surface temperature, f is the fraction of water ice in the active regions, $\alpha_{\rm R}$ accounts for the recondensation of water ice on the surface (Crifo 1987), L [J kg^{-1}] is the latent heat of sublimation of water ice, and $Z(T)$ [kg s^{-1} m^{-2}] is the H_2O sublimation rate.

For the latent heat of sublimation of water ice L, we took the standard value:

$$L = 2.8\times10^6 \ {\rm J\,kg^{-1}}. \quad (6)$$

The H_2O sublimation rate $Z(T)$ is given by:

$$Z(T) = P_{\rm v}(T)\sqrt{\frac{M}{2\pi RT}} \quad (7)$$

where $M = 18$ g mol^{-1} is the H_2O molecular weight and $R = 8.314$ J K^{-1} mol^{-1} is the gas constant. The vapor pressure $P_{\rm v}(T)$ [Pa] is given by (Fanale and Salvail 1984):

$$P_{\rm v}(T) = A\exp\left(\frac{-B}{T}\right) \quad (8)$$

where $A = 3.56\times10^{12}$ Pa and $B = 6162$ K. The numerical values of the other parameters will be discussed in Sect. 4.4.

As heat conduction is negligible, the coordinates system does not depend on the pole orientation of the nucleus and we arbitraly chose a zero obliquity (with respect to the Sun-comet-Earth plane). Equations (4) and (5) are solved numerically and give the surface temperature distribution $T(\theta,\varphi)$ of the inactive and active regions respectively, using the relation $\cos z = \cos\theta\cos\varphi$, where θ is the latitude and φ is the longitude, measured from the subsolar point. On the night side, $T = 0$ K.

4.2. The thermal flux

The thermal flux $F(\lambda)$ of an unresolved nucleus measured by an observer located at distance Δ is the integral over the nucleus of the Planck function $B(\lambda,T)$, where $T(\theta,\varphi,p_{\rm v})$ is given by Eq. (4) or Eq. (5):

$$F(\lambda) = \epsilon\int\int B\Big[\lambda, T(\theta,\varphi,p_{\rm v})\Big]\Omega{\rm d}S. \quad (9)$$

The solid angle Ω is given by:

$$\Omega = \frac{1}{\Delta^2}\cos\theta\cos(\varphi-\alpha), \quad (10)$$

the element of surface by:

$${\rm d}S = r_{\rm n}^2\cos\theta{\rm d}\theta{\rm d}\varphi \quad (11)$$

where α is the phase angle given in Table 2. We calculated the thermal flux by performing a double integration over the hemisphere of the nucleus which is visible from the Earth i.e., satisfying $\cos(\varphi-\alpha) > 0$. This method avoids introducing an arbitrary thermal phase function.

We obtained the thermal flux $F_{\rm inact}$ from the inactive regions using the temperature distribution given by Eq. (4), and the thermal flux $F_{\rm act}$ from the active regions using the temperature distribution given by Eq. (5). The thermal flux of the nucleus $F_{\rm nucl}$ is a combination of these two thermal fluxes according to:

$$F(\lambda)_{\rm nucl} = (1-x)F_{\rm inact} + xF_{\rm act}. \quad (12)$$

The measured thermal emission from the nucleus provides a first relationship between $r_{\rm n}$ and x, assuming a value for the geometric albedo $p_{\rm v}$.

4.3. The water production rate

The water production was calculated at each point (θ,φ) of the surface, and then integrated over the whole surface. Only a fraction x of the surface is active, with a fraction f of water ice, so that $Q_{\rm H_2O}$ is given by:

$$\begin{aligned}(Q_{\rm H_2O})_{\rm total} &= r_{\rm n}^2\int_{-\pi}^{\pi}\int_{-\pi/2}^{\pi/2}Q_{\rm H_2O}(\theta,\varphi)\cos\theta{\rm d}\theta{\rm d}\varphi \\ &= r_{\rm n}^2\int_{-\pi}^{\pi}\int_{-\pi/2}^{\pi/2}xf(1-\alpha_{\rm R})Z[T(\theta,\varphi)]\cos\theta{\rm d}\theta{\rm d}\varphi. \quad (13)\end{aligned}$$

The temperature $T(\theta,\varphi)$ is given by Eq. (5). The water production rate of the nucleus provides a second relationship between $r_{\rm n}$ and x.

4.4. The parameters

The various parameters involved in the thermal model are not known for cometary nuclei. We discuss below how we selected their respective values.

The infrared emissivity ϵ is taken equal to 0.95, the middle point of the interval 0.9–1.0 always quoted in the literature. As the interval is very small and the value near 1.0, this uncertainty has a negligible impact on the calculated thermal flux.

The beaming factor η reflects the influence of the surface roughness which produces an anisotropic thermal emission. The values of η determined for a few asteroids and planetary satellites vary from 0.7 to 1.2 (Spencer et al. 1989; Harris 1998). The value of $\eta = 0.756$, derived from observations of 1 Ceres and 2 Pallas by Lebofsky et al. (1986) has often been considered a standard and used for other solar system objects (e.g., Centaur Chariklo, Jewitt & Kalas 1998). However, for low albedo objects such as cometary nuclei, Lagerros (1998) pointed out that a rather high surface roughness is required in order to achieve this value. His recommendation led us to select the more appropriate value $\eta = 0.85$. As the temperature varies as $\eta^{-1/4}$, the beaming factor has an important effect on thermal flux and, in turn, on the determination of the nuclear radius.

The Bond albedo A requires a knowledge of the phase integral q, which measures the angular dependence of the scattered radiation. We chose $q = 0.28$, the value found for 253 Mathilde (Clark et al. 1999) since the surface properties of this asteroid ($p_v = 0.047$ and $\beta_V = 0.04$ mag/deg) are typical of cometary nuclei. This choice is reinforced by the recent Deep Space 1 observations of 19P/Borrelly for which Buratti et al. (2004) derived a phase integral of 0.27 ± 0.01.

We adopted a geometric albedo $p_v = 0.04$, typical of cometary nuclei (Lamy et al. 2004). Is it not possible to directly determine this parameter for 126P/IRAS and 103P/Hartley 2, using the radiometric method (visible + infrared), as no visible observations of the nucleus are available.

The recondensation of water ice on the surface is discussed in detail by Crifo (1987). We adopted his recommended value $\alpha_R = 0.25$.

The volumic fraction of ice f in the ice-dust mixed model is set to 0.2, to insure that the geometric albedo of the nucleus is compatible with the above value of 0.04, even when the active fraction x becomes very large. It will be shown later that the results remain insensitive to the value of f in the range 0.01–1.0.

5. Properties of the nucleus

Using the constraints on the infrared flux (Eq. (12)) and on the water production rate (Eq. (13)), it is possible to independently determine the radius r_n and the active fraction x of the nucleus. Active regions are colder than inactive regions because of water ice sublimation. Consequently, the larger the active fraction x, the lower the average surface temperature, and so the larger the radius r_n to match the observed infrared flux. Moreover, the larger the active fraction x, the larger the active regions, and so the smaller the radius r_n to match the observed water production rate. The combination of these two opposite constraints allows to determine a unique solution for x and r_n. This method assumes that the active fraction remains constant between the date of the infrared observations and the date of the water production measurements. We will now apply this method to 126P/IRAS and 103P/Hartley 2.

5.1. 126P/IRAS

The infrared flux of its nucleus measured 13 days after its perihelion passage amounts to 48 ± 8 mJy (Table 2). The water production rate has been extrapolated at perihelion by A'Hearn et al. (1995) and amounts to 3.2×10^{27} molecules s^{-1}; an uncertainty of ~30 % is realistic. The time interval of 13 days is sufficiently short to assume that x did not vary much. The infrared constraint and the water production constraint are represented in Fig. 5. We derived a radius of 1.57 ± 0.14 and an active fraction of 0.11 ± 0.03 at perihelion assuming $f = 0.2$, but different values of f in the range 0.01–1 led to negligible differences on the radius (1.56–1.57 km) and small differences on the active fraction (0.09–0.13). The very small influence of f on r_n and x results from two facts:

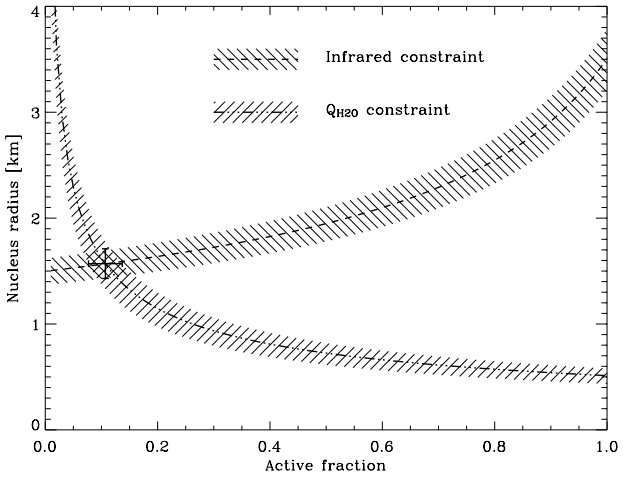

Fig. 5. The radius of the nucleus of 126P/IRAS as a function of the active fraction.

i) the active regions, whose temperature is controlled by f, contribute little to the infrared flux since they represent only 11% of the surface and since their temperature is lower than that of the inactive regions at the time of observations;
ii) for $r_h < 1.7$ AU, the bulk of the available solar energy (>85 %) is used for sublimation, implying an almost constant production rate Z.

The classical determination of the radius using the STM led to a radius of 1.50 km, very close of the above value. Consequently, the STM is applicable as long as the active fraction of a nucleus remains small. Although the active areas are colder, the resulting reduction of the infrared flux is negligible in that case.

We checked whether the variations of the flux of 126P/IRAS in Table 2 could be due to a rotational lightcurve. We applied the Lomb periodogram analysis (Press et al. 1992) to the data points, searching for double-peaked periods between 2 h and 160 h. A broad peak appears at $P = 4.9 \pm 0.9$ h in the periodogram, but it is not statistically significant, owing to the large error bars and to the limited number of data points. The measurements phased to this period are shown in Fig. 6. We note that a rotational period of ~5 h is not unrealistic for a cometary nucleus as it lies at the low end of the observed range (5–70 h, Lamy et al. 2004).

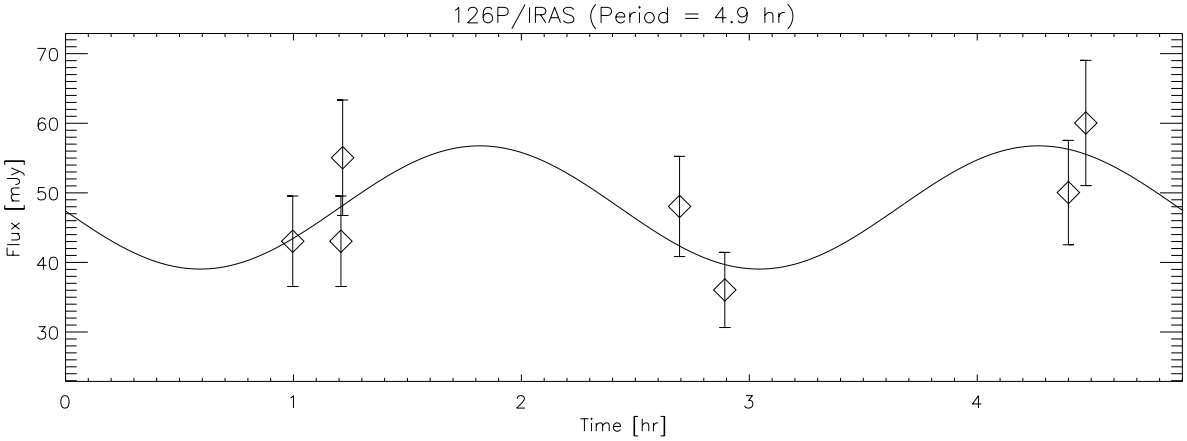

Fig. 6. Data points of Table 2 for comet 126P/IRAS phased to the most likely period of 4.9 ± 0.9 h (diamonds) and the fitted sine curve (solid line). Note that this period is not statistically significant in the Lomb periodogram.

Table 3. Measured water production rates for 103P/Hartely 2.

Date	r_h [AU]	Q_{H2O} [10^{28} molecules/s]	$x^\dagger$	Ref.
1997 passage (q = 1.03 AU)				
31 Dec. 1997	1.04	1.24 ± 0.20	0.58 ± 0.20	(1)
01 Jan. 1998	1.04	3.1 ± 0.2	1.44 ± 0.50	(2)
19 Jan. 1998	1.11	0.54 ± 0.20	0.30 ± 0.11	(1)
1991 passage (q = 0.95 AU)				
11 Sep. 1991	0.95	4.5‡	1.71 ± 0.60	(3)
16–22 Sep. 1991	0.96	6.3	2.44 ± 0.85	(4)

† Active fraction for a radius of 0.71 km with an uncertainty of 35% (see text for detail);
‡ this value at perihelion has been extrapolated from OH production rates measured on 9–12 Oct. 1991, corresponding to the interval 1.03–1.05 AU post-perihelion.
References – (1) Crovisier et al. (1999), (2) Colangeli et al. (1999), (3) A'Hearn et al. (1995), (4) Weaver et al. (1994).

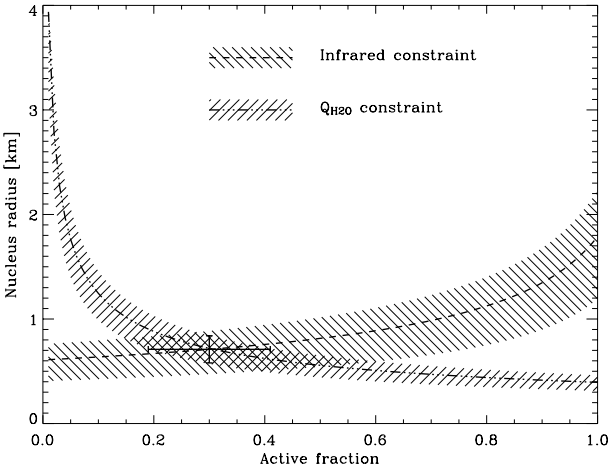

Fig. 7. The radius of the nucleus of 103P/Hartley 2 as a function of the active fraction.

5.2. 103P/Hartley 2

The infrared flux of its nucleus measured 46 days after its perihelion passage amounts to 27 ± 15 mJy (Table 2). Several water production rates have been obtained for 103P/Hartley 2, summarized in Table 3. We used the measurement of Croviser et al. (1999) at 1.11 AU which is the closest to our ISOCAM observation (16 days before). The infrared constraint and the water production constraint are represented in Fig. 7. We obtained a radius of 0.71 ± 0.13 km and an active fraction of 0.30 ± 0.11 assuming f = 0.2. The influence of f in the range 0.01–1 is nil on r_n and very small on x (0.28–0.32). However, we note that the real water production rate at 1.21 AU, during the ISOCAM observations, may be slightly smaller than the adopted value measured by Crovisier et al. (1999) at 1.11 AU.

The STM which corresponds to Q_{H2O} = 0 yields a radius of 0.61 km, a lower limit not very different from our above determination of 0.71 km. Even for an active fraction as large as 30%, it thus appears that the STM gives a correct approximation.

From our determination of the radius of 0.71 km, it is possible to estimate the active fraction x for every water production rate given in Table 3. We assume an uncertainty of 35% on x, consistent with our own error bar (x = 0.30 ± 0.11). The measurement of Crovisier et al. (1999) at 1.04 AU leads to x = 0.58 ± 0.20, while that of Colangeli et al. (1999) leads to x = 1.44 ± 0.50 at the same heliocentric distance. Clearly this discrepancy comes from the 2.5 factor between the two rates, a question not settled by the authors. For all three observations at the 1997 passage, the active fraction is less than 1 at the 1 σ level. For the 1991 passage, the nominal values of x exceed 1 but only by 1.2 σ for the first value x = 1.71 ± 0.60 and by 1.7 σ for the second value x = 2.44 ± 0.85. We consider that these excesses are not statistically significant and that our result is rather quite satisfactory in view of the large scatter of the water production rates which probably results from the different methods used by the different groups. We conclude that the radius of the nucleus of 103P/Hartley 2 is 0.71 ± 0.13 km and that its active fraction reaches ∼100% at perihelion, in agreement with the absence of structure in the coma.

Such a small, very active nucleus would be extremely difficult to detect from the ground. Indeed observations at

r_h = 3.63 AU post-perihelion by Lowry and Fitzsimmons (2001) and further away at r_h = 4.73 AU post-perihelion by Licandro et al. (2000) have shown that it was still active in both cases. The above authors could therefore obtain only upper limits for the radius of the nucleus, respectively <5.9 and ≪5.0 km.

5.3. Discussion

As demonstrated above, the Standard Thermal Model widely implemented to derive the radius of cometary nuclei from infrared observations is well adapted to low active nuclei, i.e., for active fraction ≤0.3. Indeed for 126P/IRAS and 103P/Hartley 2, the difference between the two determinations of the radius (STM and our method) amounts to 5–15%. This difference increases with the active fraction: for fractions of 60%, 80% and 100%, the STM underestimates the radius by factors of respectively 1.5, 1.9 and 3.5 at 1 AU, 1.3, 1.4 and 1.6 at 2 AU and less than 1.2 at 3 AU. Clearly the difference tends to vanish as the heliocentric distance increases, a result of the vanishing difference bewteen the temperature of active and inactive regions. The importance of the active fraction must not be underestimated as widespread activity over the nucleus appears to be common among ecliptic comets such as 46P/Wirtanen with $x \sim 85\%$ at perihelion (Groussin & Lamy 2003a) and 22P/Kopff with $x > 0.35$ (Lamy et al. 2002); application of the STM may therefore lead to substantial errors on the determination of the radius of the nucleus.

6. Conclusions

We have presented a coherent method which, for the first time, allows us to simultaneously analyze thermal infrared observations of the nucleus and measurements of the water production rate to determine, in a self consistent way, its radius and its active fraction. Our thermal model assumes a spherical nucleus covered by a mosaic of small and numerous active and inactive regions and takes into account all first order physical processes. We have applied this method to two quite different comets, 126P/IRAS and 103P/Hartley 2 and have obtained the following results:

i) a radius of 1.57 ± 0.14 km and an active fraction of 0.11 ± 0.03 at perihelion, for the nucleus of 126P/IRAS;
ii) a radius of 0.71 ± 0.13 km and an active fraction of ∼1 at perihelion and 0.30 ± 0.11 at 1.11 AU post-perihelion, for the nucleus of 103P/Hartley 2, which is therefore one more example of a small, very active nucleus, very similar to that of 46P/Wirtanen (Lamy et al. 1998a; Groussin & Lamy 2003a).

We have further shown that the standard thermal model is applicable to low activity nuclei. Typically it will underestimate the radius by ∼15% if the active fraction is about 0.30. For very active nuclei, observed inside 2 AU, the STM may lead to larger errors, e.g. a factor ≥1.4 for active fractions $x \geq 0.8$. This is very important as many ecliptic comets appear to display widespread activity, consistent with the absence of structure in their coma.

The two comets studied here confirm the wide diversity of the activity pattern on cometary nuclei, from a few active vents covering only a few percent of the surface (e.g., 1P/Halley (Keller 1997), 19P/Borrelly (Lamy et al. 1998b), 109P/Swift-Tuttle (Sekanina 1981), C/1995 O1 Hale-Bopp (Schleicher et al. 1997)) to fairly extended activity (e.g., 22P/Kopff, with $x \geq 0.35$ (Lamy et al. 2002)) to generalized activity pretty much over the bulk of the nucleus surface (e.g., 46P/Wirtanen, with $x \sim 0.85$ (Groussin & Lamy 2003a), 103P/Hartley 2 with $x \sim 1$).

Acknowledgements. We are grateful to the ISO operators and support staff at ESA-Vilspa. We acknowledge the assistance of M. Sauvage and O. Laurent of the ISOCAM team at CEA. This work was supported by a grant from the "Programme National de Planétologie" funded by CNRS and CNES. I. Toth acknowledges financial support from the Université de Provence. The ISOCAM data presented in this paper were analyzed using "CIA", a joint development by the ESA Astrophysics Division and the ISOCAM Consortium. We thank the anonymous referee for many helpful comments.

References

A'Hearn, M. F., Millis, R. L., Schleicher, D. G., Osip, D. J., & Birch, P. V. 1995, Icarus, 118, 223
Buratti, B. J., Hicks, M. D., Oberst, J., et al. 2004, Deep Space 1 photometry of the nucleus of comet 19P/Borrelly, Icarus, 167, 16
Carusi, A., Kresak, L., Perozzi, E., & Valsecchi, G. B. 1985, Long-term evolution of short-period comets (Bristol, UK and Accord, M.A.: Adam Hilger, Ltd.), 272
Cesarsky, C. J. 1994, Exp. Astron., 3, 101
Cesarsky, C. J., Abergel, A., Agnese, P., et al. 1996, A&A, 315, L32
Clark, B. E., Veverka, J., Helfenstein, P., et al. 1999, Icarus, 140, 53
Colangeli, L., Epifani, E., Brucato, J. R., et al. 1999, A&A, 343, L87
Crifo, J. F. 1987, A&A, 187, 438
Crifo, J. F., & Rodionov, A. V. 1997, Icarus, 127, 319
Crovisier, J., Encrenaz, Th., Lellouch, E., et al. 1999, ESA SP-427
Davies, J., Green, S., Stewart, B., et al. 1983, IAUC, 3796
Fanale, F. P., & Salvail, J. R., 1984, Icarus, 60, 476
Fernández, Y. R., Lisse, C. M., Ulrich Käufl, H., et al. 2000, Icarus, 147, 145
Fernández, Y. R., Jewitt, D. C., & Sheppard, S. S. 2002, AJ, 123, 1050
Groussin, O., & Lamy, P. 2003a, A&A, 412, 879
Groussin, O. 2003b, Ph.D. Thesis, Université Aix-Marseille II, France
Groussin, O., Lamy, P., & Jorda, L. 2004, A&A, 413, 1163
Harris, A. W. 1998, Icarus, 131, 291
Hartley, M. 1984, IAUC, 4015
Jewitt, D., & Kalas, P. 1998, ApJ, 499, L103
Jorda, L., Lamy, P. L., Toth, I., et al. 2000, ESA SP-455, 61
Keller, H. U., & Thomas, N. 1997, Adv. Space Res., 19, 187
Lagerros, J. S. V. 1998, A&A, 332, 1123
Lamy, P. L., & Toth, I. 1995, A&A, 293, L43
Lamy, P. L., Toth, I., Grun, E., et al. 1996, Icarus, 119, 370
Lamy, P. L., Toth, I., Jorda, L., & Weaver, H. A. 1998a, A&A, 335, L25
Lamy, P. L., Toth, I., & Weaver, H. A. 1998b, A&A, 337, 945
Lamy, P., Jorda, L., Toth, I., et al. 1999, BAAS, 31, 27-03
Lamy, P., Toth, I., Jorda, L., et al. 2002, Icarus, 156, 442
Lamy, P., Jorda, L., Groussin, O., et al. 2004, The nucleus of comet 55P/Tempel-Tuttle and its inner coma, Icarus, submitted
Lamy, P. L., Toth, I., Fernandez, Y., & Weaver, H. A. 2004, COMETS II, ed. M. Festou, H. U. Keller, & H. A. Weaver (The University of Arizona Press), in press

Lebofsky, L. A., Sykes, M. V., Tedesco, E. F., et al. 1986, Icarus, 68, 239
Levison, H. F. 1996, Completing the Inventory of the Solar System ASP, ed. T. W. Rettig, & J. M. Hahn, ASP Conf. Proc., 107, 173
Licandro, J., Tancredi, G., Lindgren, M., Rickman, H., & Hutton, R. G. 2000, A&A, 147, 161
Lisse, C. M., Fernández, Y. R., Kundu, A., et al. 1999, Icarus, 140, 189
Lowry, S. C., & Fitzsimmons A. 2001, A&A, 365, 204
Press, W. H., Teukolsky, S. A., Vetterling, W. T., & Flannery, B. P. 1992, Numerical Recipes, 2nd ed. (Cambridge University Press)
Schleicher, D. G., Lederer, S. M., Millis, R. L., & Farnham, T. L. 1997, Science, 275, 1913
Sekanina, Z. 1981, AJ, 86, 1741
Siebenmorgen, R., Starck, J.-L., Sauvage, M., et al. 1998, ISOCAM Data User Manual Version 4.0, SAI/95-222/Dc
Siebenmorgen, R., Blommaert, J., Sauvage, M., & Starc, J.-L. 1999, ISO Handbook III (CAM), Draft version 1.0, SAI/99-057/Dc
Spencer, J. R., Lebofsky, L. A., & Sykes, M. V. 1989, Icarus, 78, 337
Weaver, H. A., Feldman, P. D., McPhate, et al. 1994, ApJ, 422, 374
Weaver, H. A., & Lamy, P. L. 1999, EM&P, 79, 17